



RESEARCH LETTER

10.1029/2022GL102493

Projected Changes in Hot, Dry, and Compound Hot-Dry Extremes Over Global Land Regions

Paolo De Luca¹ and Markus G. Donat^{1,2} ¹Barcelona Supercomputing Center (BSC), Barcelona, Spain, ²Institució Catalana de Recerca i Estudis Avançats (ICREA), Barcelona, Spain

Key Points:

- Hot extremes are projected to increase in frequency and intensity over almost all land areas by the end of the 21st century
- Drought changes depend on measure but increase robustly over central and northern South America, the Mediterranean, and southern Africa
- Compound hot and dry extremes are sensitive to the drought measure but projected to increase in most regions globally

Supporting Information:

Supporting Information may be found in the online version of this article.

Correspondence to:

P. De Luca,
paolo.deluca@bsc.es

Citation:

De Luca, P., & Donat, M. G. (2023). Projected changes in hot, dry, and compound hot-dry extremes over global land regions. *Geophysical Research Letters*, 50, e2022GL102493. <https://doi.org/10.1029/2022GL102493>

Received 3 JAN 2023

Accepted 18 MAY 2023

Author Contributions:

Conceptualization: Paolo De Luca, Markus G. Donat
Data curation: Paolo De Luca
Formal analysis: Paolo De Luca
Funding acquisition: Markus G. Donat
Investigation: Paolo De Luca
Methodology: Paolo De Luca, Markus G. Donat
Project Administration: Markus G. Donat
Supervision: Markus G. Donat
Validation: Paolo De Luca
Visualization: Paolo De Luca
Writing – original draft: Paolo De Luca

© 2023 The Authors.

This is an open access article under the terms of the [Creative Commons Attribution-NonCommercial License](https://creativecommons.org/licenses/by-nc/4.0/), which permits use, distribution and reproduction in any medium, provided the original work is properly cited and is not used for commercial purposes.

Abstract The impacts of hot, dry, and compound hot-dry extremes are significant for societies, economies, and ecosystems worldwide. Such events therefore need to be assessed in the light of anthropogenic climate change so that suitable adaptation measures can be implemented by governments and stakeholders. Here we show a comprehensive analysis of hot, dry, and compound hot-dry extremes over global land regions using 25 Coupled Model Intercomparison Project Phase 6 models and four future emissions scenarios from 1950 to 2100. Hot, dry, and compound hot-dry extremes are projected to increase over large parts of the globe by the end of the 21st century. Hot and compound hot-dry extremes show the most widespread increases and dry extreme changes are sensitive to the index used. Many regional changes depend on the strength of greenhouse-gas forcing, which highlights the potential to limit the changes with strong mitigation efforts.

Plain Language Summary Heatwaves, drought and their joint occurrences can negatively impact populations, economies, and natural systems worldwide. It is therefore of paramount importance that governments and stakeholders assess the risk from such events and adapt accordingly. In this study we use 25 climate models and four emission scenarios from 1950 to 2100 to assess how hot, dry, and compound hot-dry extremes are expected to change in the future when compared to current climate conditions. We find that such extremes are projected to increase by the end of the 21st century over large parts of global land areas under the highest-emission, no-policy, climate change scenario. Hot and compound hot-dry extremes show the most widespread increases, whereas dry extreme changes are sensitive and more regionally limited depending on the method by which they are computed. Most of the regional changes in hot, dry, and compound hot-dry extremes can be reduced with strong climate change mitigation efforts to limit future greenhouse gas emissions.

1. Introduction

Socio-economic and environmental impacts of hot, dry, and compound hot-dry meteorological extremes can pose a significant distress to natural and socio-economic systems worldwide (Barriopedro et al., 2011; Zscheischler & Fischer, 2020; Zscheischler et al., 2018). It is therefore of paramount importance to provide information on how these meteorological hazards may change in the future under anthropogenic climate change.

Hot and dry extremes can occur concurrently (or within a time-frame of a few weeks) at a location (Bevacqua et al., 2022; Hao et al., 2018; Manning et al., 2019; Mukherjee et al., 2022, 2023; Zscheischler et al., 2018, 2020) and at present, there are no metrics for computing compound hot-dry extremes which gathered the same importance as for example, the Climpact indices for univariate extremes (<https://climpact-sci.org/>). This is because research on compound extremes is a relatively new field of investigation and also because compound events can be quantified in many different ways, for example, occurring simultaneously or subsequently, at the same location or at different locations (e.g., De Luca, Messori, Pons, Faranda, 2020; De Luca, Messori, Wilby, et al., 2020), so that the analysis remains complex, hindering a broader consensus about which aspect of compound extremes matters most for a certain application. However, some studies developed pragmatic indices and metrics for hot-dry extremes. Examples are X. Wu et al. (2019) who developed a dry-hot magnitude index, Zhang et al. (2022) who assessed compound agricultural droughts and hot events, Bevacqua et al. (2022) who defined compound hot-dry events based on temperature and precipitation mean values within the warm season and Ganguli (2023) who explored compound warm-dry events in India by developing an index based on (warm) temperature, (lack of) precipitation and (low) wind-speed.

There is now a general consensus about a global increase in hot extremes under anthropogenic climate change (e.g., Christidis et al., 2015; Fischer & Schär, 2010; Perkins-Kirkpatrick & Lewis, 2020), with such trend mainly

Writing – review & editing: Paolo De Luca, Markus G. Donat

attributed to thermodynamic changes, or to an increase in global mean temperature (Rastogi et al., 2020; Vogel, Zscheischler, et al., 2020) and local land-atmosphere feedbacks (Donat et al., 2017; Seneviratne et al., 2006), with also changes in the atmospheric circulation playing a role for example, in Eurasia and North America (Horton et al., 2015; Rousi et al., 2022; Schielicke & Pfahl, 2022; Suarez-Gutierrez et al., 2020). Future projected changes in drought are sensitive to the index used (Cook et al., 2018; Dai, 2011, 2013). This is because drought can be computed from precipitation alone (McKee et al., 1993) and also from the combination of precipitation and potential evapotranspiration (PET) (Palmer, 1965; Vicente-Serrano et al., 2010), with the latter case taking into account the effect of increasing temperatures. Future changes in drought based on precipitation deficit point toward an increase in dryness over northern South America, the Mediterranean, southern Africa and South Australia (Ukkola et al., 2020). On the other hand, projections of drought computed from precipitation and PET show increased dryness over the same regions as Ukkola et al. (2020) and also in Central and central-north America, most of the African continent, central Europe, the Middle East, southeast Asia and Australia (Dai, 2011, 2013). Lastly, changes in drought can be also sensitive to the equation used to approximate PET, a shown in Begueria et al. (2014). Other factors playing a role in shaping drought events in the short-term over some of these regions are sea-surface temperatures anomalies, weakened summer Asian monsoons and likely changes in atmospheric circulation patterns (Dai, 2011, 2013; Schubert et al., 2016; Teuling et al., 2013; Trenberth et al., 2014). Lastly, and reflecting the changes in hot and dry extremes, also compound hot-dry extremes are set to increase under anthropogenic climate change (Bevacqua et al., 2022; Ridder et al., 2022; Vogel, Hauser, et al., 2020) and they appear to be modulated by mean precipitation trends (Bevacqua et al., 2022). Most of these studies consider hot, dry and hot-dry compound extremes separately, hindering a robust understanding of how these types of extremes relate to each other. Moreover, they do not use different metrics for the computation of dry extremes, also on several accumulation periods, such as indices that consider precipitation and precipitation along with evaporative water demand, that can in turn affect dry and compound hot-dry extreme changes.

Here we build on these works and provide a comprehensive analysis of projected changes in hot, dry and compound hot-dry extremes over global land regions. We use a multi-model ensemble (MME) of 25 Coupled Model Intercomparison Project Phase 6 (CMIP6) models (Eyring et al., 2016), four emission scenarios, and a suite of different univariate and compound extreme indices. Such indices consider different aspects of drought, such as precipitation and evaporative water demand over multiple accumulation periods, also in compound extremes, which in combination allows us to discuss how the changes in compound extremes relate to their univariate hot and dry contributions.

2. Data and Methods

2.1. Data

We use CMIP6 data (Eyring et al., 2016), namely historical and future Scenario Model Intercomparison Project (ScenarioMIP) (O'Neill et al., 2016) simulations. From the ScenarioMIP we use four Shared Socioeconomic Pathways (SSPs): SSP1-2.6, SSP2-4.5, SSP3-7.0, and SSP5-8.5. From these simulations we extract daily maximum near-surface temperature (t_{max} , K), daily minimum near-surface temperature (t_{min} , K) and daily precipitation (pr , $\text{kg}\cdot\text{m}^{-2}\cdot\text{s}^{-1}$), respectively for the periods 1950–2014 and 2015–2100, for a MME of 25 models (Table S1 in Supporting Information S1). From each model we only considered the first ensemble member available (in most cases $r1i1p1f1$) so that models' structural uncertainty is taken into account (Deser, 2020).

2.2. ClimPact Indices

We compute a selection of extreme indices to quantify global hot and dry extremes from 1950 to 2100, using 1981–2010 as a baseline period for the calculation of percentile thresholds. The indices are computed starting in 1949 to avoid obtaining incomplete index calculations in 1950 for indices that accumulate across calendar years, namely the Standardized Precipitation Index (SPI, McKee et al., 1993) and Standardized Precipitation Evapotranspiration Index (SPEI, Vicente-Serrano et al., 2010). For hot extremes we calculate the percentage of days when daily maximum temperature exceeds the 90th percentile ($tx90p$) and the annual maximum of daily maximum temperatures (txx) (Zhang et al., 2011). We also calculate three indices measuring heatwave characteristics, where heatwaves are considered as periods of at least three consecutive days when daily maximum temperatures exceed the 90th percentile (Perkins & Alexander, 2013). The heatwave amplitude (hwa_{tx90}) represents the annual peak

daily value ($^{\circ}\text{C}$) in the hottest heatwave, the heatwave duration (hwd_{tx90}) refers to the length (days) of the longest heatwave within a year and heatwave frequency (hwf_{tx90}) measures the number of days within a year that contribute to heatwaves (<https://climimpact-sci.org/>).

To quantify the occurrence of dry extremes we use the SPI and SPEI with 3-, 6-, and 12-month accumulation periods. The SPI provides information about meteorological drought in terms of lack of precipitation, whereas the SPEI in terms of lack of water availability by considering also the atmospheric water demand. SPI and SPEI include the entire precipitation, or precipitation minus PET, distributions, and do not directly indicate drought occurrences. A caveat is that PET may overestimate drought in very dry regions, where actual evapotranspiration may be lower than PET due to lack of water. We define drought when these monthly index values are ≤ -1 , which represents moderate drought conditions. We use -1 as threshold to ensure a sufficient number of monthly values within the SPI and SPEI drought data sets, but lower values could be used as criterion for more severe drought. As a baseline for the estimation of the distribution parameters we use the entire investigation period (151 years, 1950–2100) (Vicente-Serrano et al., 2020), to avoid potential biases outside relatively short reference periods as reported for example, by Sippel et al. (2015). To allow comparison across SSPs, we use the SPI and SPEI distribution parameters derived for the Historical and one SSP scenario (i.e., SSP1-2.6) to compute SPI and SPEI in the other scenarios. We use SSP1-2.6 because this is the scenario with smallest forcing changes. For the SPEI we compute PET following Hargreaves (1994), which is based on maximum and minimum temperatures (K), and latitude to estimate extraterrestrial radiation. SPEI results can be sensitive to how PET is calculated (e.g., Beguería et al., 2014). Therefore, we assess the sensitivity of SPEI to different PET approximations, that is, following Thornthwaite (1948), and the more complex Penman method (Allen et al., 1994). We perform this comparison for two CMIP6 models, under SSP5-8.5 and SSP2-4.5, for $spei3$, $spei6$ and $spei12$. We find that annual global mean time-series are in agreement between the Hargreaves and Penman methods, but using the Thornthwaite method results in much stronger drying (Figures S1 and S2 in Supporting Information S1). Similarly, for the drought occurrence measured as $spei3_{dry}$, $spei6_{dry}$, and $spei12_{dry}$ there is good agreement between calculations using the Hargreaves and Penman methods, but a stronger and more wide-spread increase in drought occurrence is found with the Thornthwaite method (Figures S3–S6 in Supporting Information S1). For the analysis of the full MME we therefore calculate PET using the Hargreaves method which gives relatively similar results to the more complex Penman approximation but requires less data. We use the index names $spiN_{dry}$ and $speiN_{dry}$ to refer to the count of dry months, where N stands for the accumulation period of the index (i.e., 3, 6, and 12 months).

2.3. Compound Extremes

We also compute indices that measure the occurrence of (same-day) compound hot-dry extremes. We define this index as cex_d , which stands for “compound extreme days.” Here we use tasmax extremes exceeding the 90th percentile (similar to $tx90p$, as indicator for hot extremes), SPI and SPEI (3, 6, and 12-month) monthly values ≤ -1 (as indicator for dry extremes). The tasmax percentiles are computed from SSP1-2.6 during the entire 1950–2100 period, to make it consistent with the SPI and SPEI baselines, and serve as threshold for extreme temperatures in all SSP scenarios. In order to homogenize the temporal frequencies of the datasets, the SPI and SPEI original monthly time-series are converted into daily time-series by setting each daily value to the SPI and SPEI monthly value in which the day occurs.

The cex_d index assesses the occurrence of same-day compound hot-dry extremes and is computed as follows: (a) identify daily hot extremes (tasmax >90 th percentile) and daily dry extremes (SPI and SPEI ≤ -1); (b) count the number of days with compound (same-day) hot-dry extremes or when the hot days coincide with the occurrence of dry days. We name compound extremes calculated with SPI ≤ -1 as $cex_d(spiN)$ and compound extremes computed with SPEI ≤ -1 as $cex_d(speiN)$, where N stands for the number of accumulated months (i.e., 3, 6, or 12).

2.4. Statistical Analysis

We calculate all the indices on the native CMIP6 model grids and then re-grid them to a common latitude-longitude grid of $2^{\circ} \times 2^{\circ}$ so that MME medians and percentiles can be computed across all models. We then remove the ocean grid-points with a land-sea mask in order to retain only land values and exclude Antarctica. Then, for each

index we compute the MME median along with the MME interquartile range (25th and 75th percentiles), the latter used as a measure of inter-model uncertainty.

To discuss the projected changes in extremes, we present annual global average time-series (weighted by grid-point area) and maps of end-of-century changes relative to recent climate conditions. In the former we assess the MME medians using the modified Mann-Kendall test that takes into account autocorrelation (Hamed & Ramachandra Rao, 1998) and also compute the Sen's slopes of the time-series (Sen, 1968). From the modified Mann-Kendall test we extract the p -values of the MME median trends. We calculate the maps of changes by taking the difference of MME medians (computed from single-model 20-year averages) between two periods, namely the four future SSPs during 2081–2100 and the historical simulations during 1981–2000. We assess the statistical significance of the resulting end-of-century changes, for each grid-point, with a two-tailed Wilcoxon rank-sum test (Mann & Whitney, 1947) that assesses if the median values are significantly different and does not assume data normally distributed. Then, we further correct the p -values obtained with a Bonferroni correction (Bonferroni, 1936; Sedgwick, 2014) that takes into account Type I errors (or false positives) in relation to multiple testing.

As a further assessment to indicate the robustness of the simulated changes across models, we also apply a sign-test, which tests for each gridpoint if at least 80% ($n = 20$) of models have a difference value of the same sign (positive or negative).

3. Simulated Changes in Extremes

3.1. Hot Extremes

The difference maps for SSP5-8.5 show widespread significant ($p < 0.05$) increases in the different hot extremes indices, consistent with a warming climate (Figures 1a, 1c, 1e, 1g, and 1i). The $tx90p$ index shows pronounced increase in the frequency of hot extremes over northern South America, western, central and eastern Africa, the Arabian peninsula, the Tibetan plateau and Indonesia (Figure 1a), whereas txx shows largest increases in the intensity of hot extremes over central South America, central north America and Europe (Figure 1c). The hwa_tx90 shows global relatively homogeneous patterns of increased heatwave amplitude, however with largest increases over central north America, parts of Brazil and Europe (Figure 1e). The hwd_tx90 index points toward substantial increase in the duration of heatwaves over northern Africa and the Arabian peninsula (Figure 1g), whereas the hwf_tx90 index shows overall large increases in heatwave frequency, especially over northern and central parts of South America, northern Africa, the Arabian peninsula and Indonesia (Figure 1i). Similar spatial patterns of projected changes by the end of the 21st century, although less pronounced in terms of statistical significance and magnitude, are obtained for the other SSP scenarios (Figure S7–S11 in Supporting Information S1). The smaller increases in the lower-forcing scenarios (i.e., SSP1-2.6, SSP2-4.5, and SSP3-7.0) point out the benefits of implementing strong mitigation measures (O'Neill et al., 2016). Looking at the global average time-series, the MME of historical climate simulations shows relatively slow increase during the late 20th and early 21st centuries, as compared to the future high-forcing SSP scenarios. The historical simulations also show substantial reductions for the duration of 1–2 years in particular in the global average intensity of heat extremes (e.g., txx and hwa_tx90) in response to, for example, the Pinatubo volcanic eruption in 1991 (Figures 1b, 1d, 1f, and 1j). In the future projections, all indices point toward increases in hot extremes, with SSP5-8.5 being the scenario with most pronounced increases, SSP1-2.6 being the one with more moderate changes, and SSP2-4.5 with SSP3-7.0 lying between the two (Figures 1b, 1d, 1f, 1h, and 1j, $p < 0.01$, Table S2 in Supporting Information S1)—indicating proportionality between the magnitude of change and the strength of the forcing (Seneviratne et al., 2016).

3.2. Drought

Results for global dry extremes (Figure 2) differ depending on index, and therefore atmospheric variables taken into consideration, as also shown by Cook et al. (2018). The end-of-century changes for $spi3_dry$ under SSP5-8.5 point toward both drying and wetting in different regions across the globe, reflecting for example, annual mean precipitation changes reported by the IPCC AR6 (Masson-Delmotte et al., 2021; Figure SPM.5c). Hence, we find a significant ($p < 0.05$ and sign-test $>80\%$) projected increase in drought occurrence (based on SPI) in central and South America, the Mediterranean basin and southern Africa. Whereas drought occurrence is projected to decrease over central Africa, India, China and in high northern latitudes (e.g., Alaska, Canada, Scandinavia,

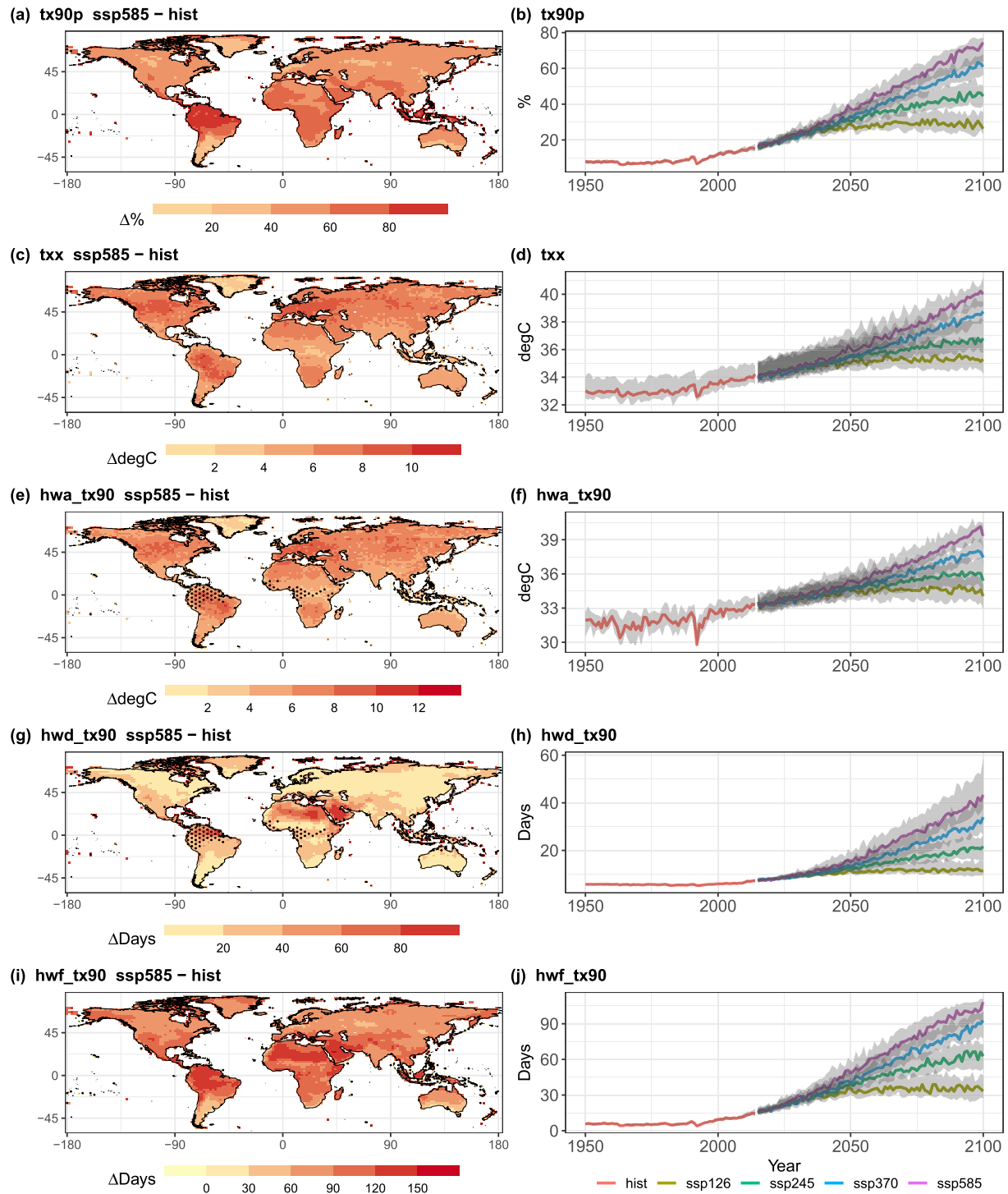


Figure 1. Multi-model ensemble (MME) difference maps and global land average time-series of hot extremes. Maps show MME median changes between the SSP8-8.5 2081–2100 and historical 1981–2000 time slices, and time-series show MME medians (colored lines) and interquartile ranges (gray shading) for the historical and Shared Socioeconomic Pathway scenarios. (a–b) *tx90p*; (c–d) *txx*; (e–f) *hwa_tx90p*; (g–h) *hwd_tx90p*; and (i–j) *hwf_tx90p*. In (a, c, e, g, and i) stippling indicates gridpoints where the difference is not statistically significant ($p \geq 0.05$) or that did not pass the sign-test ($\leq 80\%$).

and Russia; Figure 2a). Such heterogeneity in the difference maps is reflected in the global average time-series, which show a non-linear trend that cannot be assessed with a Slope value (Figure 2b). Specifically, the *spi3_dry* values of the historical period increase from 1950 to about the 1970s and then decrease until the end of the

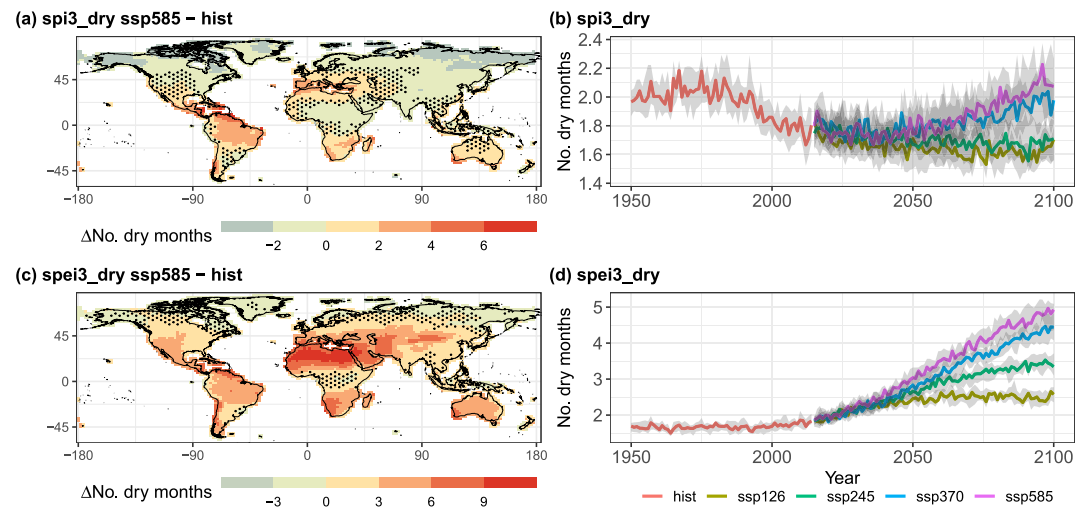


Figure 2. Multi-model ensemble difference maps and global land average time-series of dry extremes. (a–b) Annual count of dry months computed with Standardized Precipitation Index 3-month index (*spi3_dry*); (c–d) annual count of dry months computed with Standardized Precipitation Evapotranspiration Index 3-month index (*spei3_dry*). Time-periods, stippling, and time-series colors are as in Figure 1.

historical forcing runs in 2014. Following the historical period the global average *spi3_dry* values for SSP5-8.5 and SSP3-7.0 increase until the end of the 21st century, with the former showing the strongest upward trend, while the SSP2-4.5 and SSP1-2.6 global average time series remain relatively stationary (Figure 2b). However, although some global average time-series are showing little changes, the regional patterns of drying and wetting still remain in place (Figures S12 and S13 in Supporting Information S1), but compensate each other in the global average. The results suggest that at stronger forcing levels (SSP5-8.5 and SSP3-7.0) the drought increases found in some tropical and subtropical regions overcompensate the drought decreases in the high northern latitudes.

The picture is different when considering the count of dry months computed from SPEI and therefore by taking into account PET along with precipitation (*spei3_dry*; Figures 2c and 2d). Here, the end-of-century changes for SSP5-8.5 project a drying over much larger areas compared to SPI-based drought, with regions such as northern Africa, the Mediterranean, the Middle East and central China being the most affected, while only very small regions in high northern latitudes show decreases in drought occurrence based on this measure (Figure 2c). This much wider spread of drought increases is also reflected in the global average time series, which show upward trends from about 2015 to 2100 under all scenarios, with SSP5-8.5 being the one with the largest increases and SSP1-2.6 becoming stationary from about the 2050s. The other two scenarios, SSP3-7.0 and SSP2-4.5, lie between the two (Figure 2d, Table S3 in Supporting Information S1), again indicating a proportionality of the global drought response to the strength of forcing. Such a larger increase in dryness from *spei3_dry* compared to *spi3_dry* is expected as with warming temperatures also the atmospheric water demand increases (e.g., Pall et al., 2007).

The difference maps for the other *spi3_dry* and *spei3_dry* SSP scenarios have similar spatial patterns as shown in Figures 2a and 2c. However, from SSP3-7.0 to SSP1-2.6, we note that for *spi3_dry* the areas with decreasing drought occurrences increase (Figure S12 in Supporting Information S1), whereas for *spei3_dry* the areas with increasing drought counts decrease in scenarios with weaker forcing (Figure S13 in Supporting Information S1).

The difference maps for *spi6_dry*, *spei6_dry*, *spi12_dry* and *spei12_dry* show very similar patterns as found in Figures 2a and 2c, however the statistical significance is sometimes lower, especially for the *spi12_dry* and *spei12_dry* (Figures S14-S17 in Supporting Information S1). The global average time-series computed for the same dry extremes indices are also very similar to those found for *spi3_dry* and *spei3_dry* (Figure S18, Table S3 in Supporting Information S1).

3.3. Compound Hot-Dry Extremes

The end-of-century changes for compound hot-dry extremes, under the SSP5-8.5 show a widespread increase in the occurrence of such events (Figures 3a and 3c). For *cex_d (spi3)* the regions showing stronger increase in

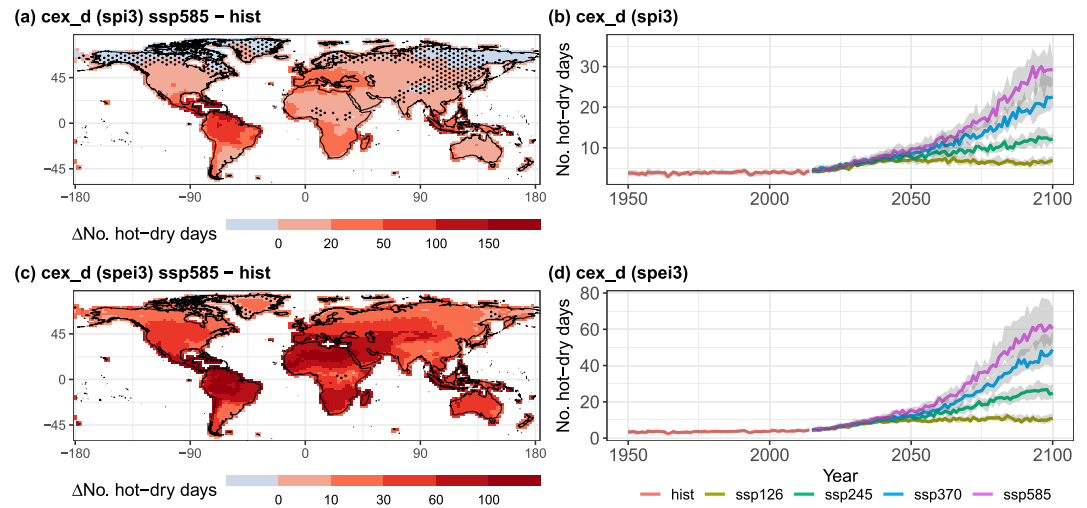


Figure 3. Multi-model ensemble difference maps and global land average time-series of compound hot-dry extremes. (a–b) Annual number of compound hot-dry extremes computed with daily maximum near-surface temperature and SPI3. (c–d) same as (a–b) but with SPEI3. Time-periods, stippling and time-series colors are as in Figure 1.

compound hot-dry extremes are central and northern South America, central Europe, the Mediterranean, western and southern Africa and Indonesia (Figure 3a). Compound hot-dry extremes computed with $cex_d(spei3)$ show large increases over the same areas mentioned above but also in northern Africa, the Middle East, and Australia (Figure 3c). For $cex_d(spi3)$ there are areas in high northern latitudes with no increase in compound extremes and this is related to the decreased drought frequency in these regions (Figures 3a and 2a). On the other hand, $cex_d(spei3)$ shows significant increases globally (Figure 3b). When looking at the climatologies (1981–2010) of compound hot-dry extremes for both $cex_d(spi3)$ and $cex_d(spei3)$ we notice that the regions where compound extremes occur more frequently under current conditions do not necessarily match with the regions where we obtain larger changes by the end of the 21st century (Figures 2a and 2c; Figures S19 and S20 in Supporting Information S1).

In accordance with the difference maps of both $cex_d(spi3)$ and $cex_d(spei3)$, also the median of annual and global average time-series show strong monotonic and positive trends for all the SSP scenarios from about 2015 to 2100, except for the SSP1-2.6 in which the compound extreme occurrences stabilize around the 2050s ($p < 0.01$, Table S4 in Supporting Information S1). As for the univariate extremes presented in the previous sections, the SSP5-8.5 is the scenario with the strongest increases, followed by SSP3-7.0, SSP2-4.5 and SSP1-2.6 (Figures 3b and 3d) and changes in compound extremes computed with SPEI to detect drought are much stronger than extremes computed with SPI.

The $cex_d(spi3)$ and $cex_d(spei3)$ difference maps computed for the other SSP scenarios show similar changes as for SSP5-8.5, although the magnitudes and statistical significance are reduced from SSP3-7.0 to SSP1-2.6 (Figures S21 and S22 in Supporting Information S1). Also the difference maps of $cex_d(spi6)$ ($spei6$) ($spi12$) and ($spei12$) reflect the changes similar to $cex_d(spi3)$ and ($spei3$), with both magnitude and statistical significance reduced from SSP5-8.5 to SSP1-2.6 and from $cex_d(spi12, spei12)$ to $cex_d(spi3, spei3)$ (Figures S23–S26 in Supporting Information S1). Lastly, the annual global average time-series for the other cex_d indices computed with $spi6$, $spei6$, $spi12$, and $spei12$ also show similar characteristics as $cex_d(spi3)$ and $cex_d(spei3)$ (Figure S27, Table S4 in Supporting Information S1).

4. Discussion and Conclusions

Our results show significant projected increases in the frequency, intensity and duration of hot extremes in most regions by the end of the 21st century, and these increases are strongest for the SSP5-8.5 scenario and weakest for SSP1-2.6. Such increase in hot extremes reflect the findings of other studies (e.g., Christidis et al., 2015; Fischer & Schär, 2010; Mukherjee et al., 2022; Yin et al., 2022) but can differ from other studies using different temperature extreme indices (e.g., Saeed et al., 2021).

Dry extremes, on the other hand, show different regional patterns of change depending on the index used to measure drought (i.e., SPI or SPEI). Such a difference is related to the types of variables included in the indices (e.g., precipitation or precipitation and PET) (Dai, 2011, 2013). While there is sensitivity to the specific measures to detect drought, the results are fairly robust for different drought accumulation periods (i.e., 3, 6, and 12 months). Dry extremes computed with SPI, under SSP5-8.5, increase over central and northern South America, the Mediterranean and southern Africa and decrease over central Africa, India, China and in the high northern latitudes. On the other hand, dry extremes computed with SPEI show consistent increase generally all over the globe, but especially in the Mediterranean, northern Africa, the Middle East and central China. Our results reflect the expectation that evaporative demand of the atmosphere increases at higher temperatures, and this is a driver of drought when characterized with SPEI. When assessing the global land average time-series, regional drought increases and decreases computed with SPI partly compensate each other and global average increases in drought only occur in the strongest forcing scenarios. On the other hand, the global land averages affected by drought computed with SPEI increase in all scenarios. The increase in dryness can be primarily driven by the changing patterns of precipitation (when based on SPI) and additionally by the increasing atmospheric water demand as the climate warms (when based on SPEI).

Results for compound hot-dry extremes are consistent with the changes in univariate hot and dry extremes and therefore the difference maps for SSP5-8.5 point toward widespread increases in compound hot-dry extremes for indices computed with both SPI (*cex_d (spi3)*, *cex_d (spi6)* and *cex_d (spi12)*) and SPEI (*cex_d (spei3)*, *cex_d (spei6)* and *cex_d (spei12)*). These widespread increases are therefore also reflected in the global land average time series, indicating significant increases by the end of the 21st century in all four scenarios.

Our findings allow a direct comparison between univariate and compound hot-dry extremes and are in accordance with other studies pointing toward an increase in hot-dry compound extremes under anthropogenic climate change. For instance, Bevacqua et al. (2022) found a projected increase in hot-dry extremes and assessed their uncertainty but only using precipitation as a proxy for dry events. Similarly, Hao et al. (2018) and Ridder et al. (2022) computed dry extremes only from precipitation and the latter study used Excess Heat Factor for assessing heatwaves. Our results show that there is some sensitivity in the projected changes with respect to dry and compound hot-dry extremes, attributed to the way dry extremes are measured.

Our analysis framework provides insights from considering the different univariate and compound indices in combination. In particular we find that global increases in hot extremes alone are driving the increase in compound extremes in regions where dry extremes, computed with SPI, decrease (e.g., northern Europe and China). On the contrary, compound extremes computed with SPEI (and computed with SPI in regions where drought becomes more frequent) are increasing because of the contributions of increasing both univariate hot and dry extremes. The pattern in compound extremes computed with SPI is also in agreement with Bevacqua et al. (2022), who highlighted the role of regional precipitation in driving future changes in compound hot-dry extremes. As limitations, we did not take into account models' uncertainty driven by internal climate variability (Deser, 2020) and dry extremes were computed from the SPI and SPEI indices at ≥ 3 months accumulation periods so that we may have lost the representation of short dry spells and with a 12-month accumulation, seasonality was implicitly removed.

In summary, we provide a comprehensive global analysis of compound hot-dry extreme changes in the context of the corresponding univariate hot and dry extremes for 25 CMIP6 models and four SSP scenarios. We specifically show that the entire set of extremes are projected to increase in the future under the highest emission scenario (SSP5-8.5) and that such increase could be partly mitigated under the lowest emission scenario (SSP1-2.6). We conclude that the risk of hot and dry extremes will significantly increase in the next decades in many regions, and encourage particular attention from governments and stakeholders worldwide to implement suitable adaptation measures and put into practice strong mitigation policies to limit the increases of such events.

Data Availability Statement

The CMIP6 data are freely available and have been downloaded from the Earth System Grid Federation (ESGF) website (<https://esgf-node.llnl.gov/search/cmip6/>). We compute the ClimImpact (<https://climimpact-sci.org/>) univariate extreme indices using the R packages “*climdex.pcic.ncdf*” (<https://github.com/ARCCSS-extremes/climdex.pcic.ncdf>) and “SPEI” (<https://github.com/sbegueria/SPEI>; Beguería et al., 2014).

Acknowledgments

This study is a contribution to the Horizon2020 LANDMARC project, and has been carried out with funding from this grant (Grant 869367). PDL has also received funding from the European Union's Horizon Europe Research and Innovation Programme under Grant 101059659. The authors would like to thank Margarida Samsó-Cabre for downloading, storing and reformatting the CMIP6 data used in the analyses.

References

Allen, R. G., Smith, M., Pereira, L. S., & Perrier, A. (1994). An update for the calculation of reference evapotranspiration. *IcID Bulletin*, 43(2), 35–92.

Barriopedro, D., Fischer, E. M., Luterbacher, J., Trigo, R. M., & García-Herrera, R. (2011). The Hot Summer of 2010: Redrawing the temperature record map of Europe. *Science*, 332(6026), 220–224. <https://doi.org/10.1126/science.1201224>

Beguería, S., Vicente-Serrano, S. M., Reig, F., & Latorre, B. (2014). Standardized precipitation evapotranspiration index (SPEI) revisited: Parameter fitting, evapotranspiration models, tools, data sets and drought monitoring. *International Journal of Climatology*, 34(10), 3001–3023. <https://doi.org/10.1002/joc.3887>

Bevacqua, E., Zappa, G., Lehner, F., & Zscheischler, J. (2022). Precipitation trends determine future occurrences of compound hot–Dry events. *Nature Climate Change*, 12(4), 350–355. <https://doi.org/10.1038/s41558-022-01309-5>

Bonferroni, C. (1936). In *Teoria statistica delle classi e calcolo delle probabilità* (Vol. 8, pp. 3–62). Pubblicazioni Del R. Istituto Superiore Di Scienze Economiche e Commerciali Di Firenze.

Christidis, N., Jones, G. S., & Stott, P. A. (2015). Dramatically increasing chance of extremely hot summers since the 2003 European heatwave. *Nature Climate Change*, 5(1), 46–50. <https://doi.org/10.1038/nclimate2468>

Cook, B. I., Mankin, J. S., & Anchukaitis, K. J. (2018). Climate change and drought: From past to future. *Current Climate Change Reports*, 4(2), 164–179. <https://doi.org/10.1007/s40641-018-0093-2>

Dai, A. (2011). Drought under global warming: A review. *Wiley Interdisciplinary Reviews: Climate Change*, 2(1), 45–65. <https://doi.org/10.1002/wcc.81>

Dai, A. (2013). Increasing drought under global warming in observations and models. *Nature Climate Change*, 3(1), 52–58. <https://doi.org/10.1038/nclimate1633>

De Luca, P., Messori, G., Pons, F. M. E., & Faranda, D. (2020). Dynamical systems theory sheds new light on compound climate extremes in Europe and Eastern North America. *Quarterly Journal of the Royal Meteorological Society*, 146(729), 1636–1650. <https://doi.org/10.1002/qj.3757>

De Luca, P., Messori, G., Wilby, R. L., Mazzoleni, M., & Di Baldassarre, G. (2020). Concurrent wet and dry hydrological extremes at the global scale. *Earth Syst. Dynam.*, 11(1), 251–266. <https://doi.org/10.5194/esd-11-251-2020>

Deser, C. (2020). Certain uncertainty: The role of internal climate variability in projections of regional climate change and risk management. *Earth's Future*, 8(12), e2020EF001854. <https://doi.org/10.1029/2020EF001854>

Donat, M. G., Pitman, A. J., & Seneviratne, S. I. (2017). Regional warming of hot extremes accelerated by surface energy fluxes. *Geophysical Research Letters*, 44(13), 7011–7019. <https://doi.org/10.1002/2017GL073733>

Eyring, V., Bony, S., Meehl, G. A., Senior, C. A., Stevens, B., Stouffer, R. J., & Taylor, K. E. (2016). Overview of the Coupled Model Intercomparison Project Phase 6 (CMIP6) experimental design and organization. *Geoscientific Model Development*, 9(5), 1937–1958. <https://doi.org/10.5194/gmd-9-1937-2016>

Fischer, E. M., & Schär, C. (2010). Consistent geographical patterns of changes in high-impact European heatwaves. *Nature Geoscience*, 3(6), 398–403. <https://doi.org/10.1038/ngeo866>

Ganguli, P. (2023). Amplified risk of compound heat stress-dry spells in Urban India. *Climate Dynamics*, 60(3), 1061–1078. <https://doi.org/10.1007/s00382-022-06324-y>

Hamed, K. H., & Ramachandra Rao, A. (1998). A modified Mann-Kendall trend test for autocorrelated data. *Journal of Hydrology*, 204(1), 182–196. [https://doi.org/10.1016/S0022-1694\(97\)00125-X](https://doi.org/10.1016/S0022-1694(97)00125-X)

Hao, Z., Hao, F., Singh, V. P., & Zhang, X. (2018). Changes in the severity of compound drought and hot extremes over global land areas. *Environmental Research Letters*, 13(12), 124022. <https://doi.org/10.1088/1748-9326/a9e96>

Hargreaves, G. H. (1994). Defining and using reference evapotranspiration. *Journal of Irrigation and Drainage Engineering*, 120(6), 1132–1139. [https://doi.org/10.1061/\(ASCE\)0733-9437\(1994\)120:6\(1132\)](https://doi.org/10.1061/(ASCE)0733-9437(1994)120:6(1132))

Horton, D. E., Johnson, N. C., Singh, D., Swain, D. L., Rajaratnam, B., & Diffenbaugh, N. S. (2015). Contribution of changes in atmospheric circulation patterns to extreme temperature trends. *Nature*, 522(7557), 465–469. <https://doi.org/10.1038/nature14550>

Mann, H. B., & Whitney, D. R. (1947). On a test of whether one of two random variables is stochastically larger than the other. *The Annals of Mathematical Statistics*, 18(1), 50–60. <https://doi.org/10.1214/aoms/1177730491>

Manning, C., Widmann, M., Bevacqua, E., Van Loon, A. F., Maraun, D., & Vrac, M. (2019). Increased probability of compound long-duration dry and hot events in Europe during summer (1950–2013). *Environmental Research Letters*, 14(9), 94006. <https://doi.org/10.1088/1748-9326/ab23bf>

Masson-Delmotte, V., Zhai, P., Pirani, A., Connors, S. L., Péan, C., Berger, S., et al. (2021). IPCC, 2021: Summary for policymakers. In *Climate Change 2021: The Physical Science Basis. Contribution of Working Group I to the Sixth Assessment Report of the Intergovernmental Panel on Climate Change*. Cambridge University Press.

McKee, T. B., Doesken, N. J., & Kleist, J. (1993). The relationship of drought frequency and duration to time scales. In *AMS 8th Conference on Applied Climatology*. In *Anaheim: AMS 8th Conference on Applied Climatology* (pp. 179–184).

Mukherjee, S., Mishra, A. K., Ashfaq, M., & Kao, S.-C. (2022). Relative effect of anthropogenic warming and natural climate variability to changes in Compound drought and heatwaves. *Journal of Hydrology*, 605, 127396. <https://doi.org/10.1016/j.jhydrol.2021.127396>

Mukherjee, S., Mishra, A. K., Zscheischler, J., & Entekhabi, D. (2023). Interaction between dry and hot extremes at a global scale using a cascade modeling framework. *Nature Communications*, 14(1), 277. <https://doi.org/10.1038/s41467-022-35748-7>

O'Neill, B. C., Tebaldi, C., van Vuuren, D. P., Eyring, V., Friedlingstein, P., Hurtt, G., et al. (2016). The scenario model Intercomparison project (ScenarioMIP) for CMIP6. *Geoscientific Model Development*, 9(9), 3461–3482. <https://doi.org/10.5194/gmd-9-3461-2016>

Pall, P., Allen, M. R., & Stone, D. A. (2007). Testing the Clausius–Clapeyron constraint on changes in extreme precipitation under CO₂ warming. *Climate Dynamics*, 28(4), 351–363. <https://doi.org/10.1007/s00382-006-0180-2>

Palmer, W. (1965). *Meteorological drought*. US Weather Bureau Research Papers.

Perkins, S. E., & Alexander, L. V. (2013). On the measurement of heat waves. *Journal of Climate*, 26(13), 4500–4517. <https://doi.org/10.1175/JCLI-D-12-00383.1>

Perkins-Kirkpatrick, S. E., & Lewis, S. C. (2020). Increasing trends in regional heatwaves. *Nature Communications*, 11(1), 3357. <https://doi.org/10.1038/s41467-020-16970-7>

Rastogi, D., Lehner, F., & Ashfaq, M. (2020). Revisiting recent US heat waves in a warmer and more humid climate. *Geophysical Research Letters*, 47(9), e2019GL086736. <https://doi.org/10.1029/2019GL086736>

Ridder, N. N., Ukkola, A. M., Pitman, A. J., & Perkins-Kirkpatrick, S. E. (2022). Increased occurrence of high impact compound events under climate change. *Npj Climate and Atmospheric Science*, 5(1), 3. <https://doi.org/10.1038/s41612-021-00224-4>

- Rousi, E., Kornhuber, K., Beobide-Arsuaga, G., Luo, F., & Coumou, D. (2022). Accelerated western European heatwave trends linked to more-persistent double jets over Eurasia. *Nature Communications*, 13(1), 3851. <https://doi.org/10.1038/s41467-022-31432-y>
- Saeed, F., Schleussner, C.-F., & Ashfaq, M. (2021). Deadly heat stress to become commonplace across South Asia already at 1.5°C of global warming. *Geophysical Research Letters*, 48(7), e2020GL091191. <https://doi.org/10.1029/2020GL091191>
- Schielicke, L., & Pfahl, S. (2022). European heatwaves in present and future climate simulations: A Lagrangian analysis. *Weather and Climate Dynamics Discussion*, 1–36. <https://doi.org/10.5194/wcd-2022-45>
- Schubert, S. D., Stewart, R. E., Wang, H., Barlow, M., Berbery, E. H., Cai, W., et al. (2016). Global meteorological drought: A synthesis of current understanding with a focus on SST drivers of precipitation deficits. *Journal of Climate*, 29(11), 3989–4019. <https://doi.org/10.1175/JCLI-D-15-0452.1>
- Sedgwick, P. (2014). Multiple hypothesis testing and Bonferroni's correction. *BMJ British Medical Journal*, 349, g6284. <https://doi.org/10.1136/bmj.g6284>
- Sen, P. K. (1968). Estimates of the regression coefficient based on Kendall's Tau. *Journal of the American Statistical Association*, 63(324), 1379–1389. <https://doi.org/10.1080/01621459.1968.10480934>
- Seneviratne, S. I., Donat, M. G., Pitman, A. J., Knutti, R., & Wilby, R. L. (2016). Allowable CO₂ emissions based on regional and impact-related climate targets. *Nature*, 529(7587), 477–483. <https://doi.org/10.1038/nature16542>
- Seneviratne, S. I., Lüthi, D., Litschi, M., & Schär, C. (2006). Land–atmosphere coupling and climate change in Europe. *Nature*, 443(7108), 205–209. <https://doi.org/10.1038/nature05095>
- Sippel, S., Zscheischler, J., Heimann, M., Otto, F. E. L., Peters, J., & Mahecha, M. D. (2015). Quantifying changes in climate variability and extremes: Pitfalls and their overcoming. *Geophysical Research Letters*, 42(22), 9990–9998. <https://doi.org/10.1002/2015GL066307>
- Suarez-Gutierrez, L., Müller, W. A., Li, C., & Marotzke, J. (2020). Dynamical and thermodynamical drivers of variability in European summer heat extremes. *Climate Dynamics*, 54(9), 4351–4366. <https://doi.org/10.1007/s00382-020-05233-2>
- Teuling, A. J., Van Loon, A. F., Seneviratne, S. I., Lehner, I., Aubinet, M., Heinesch, B., et al. (2013). Evapotranspiration amplifies European summer drought. *Geophysical Research Letters*, 40(10), 2071–2075. <https://doi.org/10.1002/grl.50495>
- Thornthwaite, C. W. (1948). An approach toward a rational classification of climate. *Geographical Review*, 38(1), 55–94. <https://doi.org/10.2307/210739>
- Trenberth, K. E., Dai, A., van der Schrier, G., Jones, P. D., Barichivich, J., Briffa, K. R., & Sheffield, J. (2014). Global warming and changes in drought. *Nature Climate Change*, 4(1), 17–22. <https://doi.org/10.1038/nclimate2067>
- Ukkola, A. M., De Kauwe, M. G., Roderick, M. L., Abramowitz, G., & Pitman, A. J. (2020). Robust future changes in meteorological drought in CMIP6 projections despite uncertainty in precipitation. *Geophysical Research Letters*, 47(11), e2020GL087820. <https://doi.org/10.1029/2020GL087820>
- Vicente-Serrano, S. M., Beguería, S., & López-Moreno, J. I. (2010). A multiscalar drought index sensitive to global warming: The standardized precipitation evapotranspiration index. *Journal of Climate*, 23(7), 1696–1718. <https://doi.org/10.1175/2009JCLI2909.1>
- Vicente-Serrano, S. M., Domínguez-Castro, F., McVicar, T. R., Tomas-Burguera, M., Peña-Gallardo, M., Noguera, I., et al. (2020). Global characterization of hydrological and meteorological droughts under future climate change: The importance of timescales, vegetation-CO₂ feedbacks and changes to distribution functions. *International Journal of Climatology*, 40(5), 2557–2567. <https://doi.org/10.1002/joc.6350>
- Vogel, M. M., Hauser, M., & Seneviratne, S. I. (2020). Projected changes in hot, dry and wet extreme events' clusters in CMIP6 multi-model ensemble. *Environmental Research Letters*, 15(9), 94021. <https://doi.org/10.1088/1748-9326/ab90a7>
- Vogel, M. M., Zscheischler, J., Fischer, E. M., & Seneviratne, S. I. (2020). Development of future heatwaves for different hazard thresholds. *Journal of Geophysical Research: Atmospheres*, 125(9), e2019JD032070. <https://doi.org/10.1029/2019JD032070>
- Wu, X., Hao, Z., Hao, F., Singh, V. P., & Zhang, X. (2019). Dry-hot magnitude index: A joint indicator for compound event analysis. *Environmental Research Letters*, 14(6), 64017. <https://doi.org/10.1088/1748-9326/ab1ec7>
- Yin, J., Slater, L., Gu, L., Liao, Z., Guo, S., & Gentine, P. (2022). Global increases in lethal compound heat stress: Hydrological drought hazards under climate change. *Geophysical Research Letters*, 49(18), e2022GL100880. <https://doi.org/10.1029/2022GL100880>
- Zhang, X., Alexander, L., Hegerl, G. C., Jones, P., Tank, A. K., Peterson, T. C., et al. (2011). Indices for monitoring changes in extremes based on daily temperature and precipitation data. *WIREs Climate Change*, 2(6), 851–870. <https://doi.org/10.1002/wcc.147>
- Zhang, Y., Hao, Z., Feng, S., Zhang, X., & Hao, F. (2022). Changes and driving factors of compound agricultural droughts and hot events in eastern China. *Agricultural Water Management*, 263, 107485. <https://doi.org/10.1016/j.agwat.2022.107485>
- Zscheischler, J., & Fischer, E. M. (2020). The record-breaking compound hot and dry 2018 growing season in Germany. *Weather and Climate Extremes*, 29, 100270. <https://doi.org/10.1016/j.wace.2020.100270>
- Zscheischler, J., Martius, O., Westra, S., Bevacqua, E., Raymond, C., Horton, R. M., et al. (2020). A typology of compound weather and climate events. *Nature Reviews Earth and Environment*, 1(7), 333–347. <https://doi.org/10.1038/s43017-020-0060-z>
- Zscheischler, J., Westra, S., van den Hurk, B. J. J. M., Seneviratne, S. I., Ward, P. J., Pitman, A., et al. (2018). Future climate risk from compound events. *Nature Climate Change*, 8(6), 469–477. <https://doi.org/10.1038/s41558-018-0156-3>